On the Plasmonic Photovoltaic

Syed Mubeen,[†,‡] Joun Lee,[†] Woo-ram Lee,[†] Nirala Singh,[‡] Galen D. Stucky,[†] and Martin Moskovits[†,*]

[†]Department of Chemistry and [‡]Department of Chemical Engineering, University of California, Santa Barbara, California 93106, United States

ABSTRACT

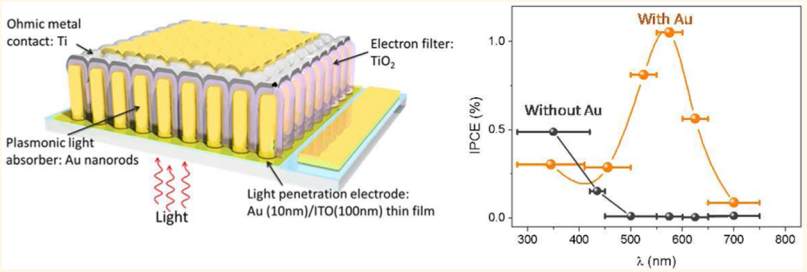

The conversion of sunlight into electricity by photovoltaics is currently a mature science and the foundation of a lucrative industry. In conventional excitonic solar cells, electron–hole pairs are generated by light absorption in a semiconductor and separated by the "built in" potential resulting from charge transfer accompanying Fermi-level equalization either at a p–n or a Schottky junction, followed by carrier collection at appropriate electrodes. Here we report a stable, wholly plasmonic photovoltaic device in which photon absorption and carrier generation take place exclusively in the plasmonic metal. The field established at a metal–semiconductor Schottky junction separates charges. The negative carriers are high-energy (hot) electrons produced immediately following the plasmon's dephasing. Some of the carriers are energetic enough to clear the Schottky barrier or quantum mechanically tunnel through it, thereby producing the output photocurrent. Short circuit photocurrent densities in the range 70–120 μA cm^{-2} were obtained for simulated one-sun AM1.5 illumination with devices based on arrays of parallel gold nanorods, conformally coated with 10 nm TiO_2 films and fashioned with a Ti metal collector. For the device with short circuit currents of 120 μA cm^{-2}, the internal quantum efficiency is ~2.75%, and its wavelength response tracks the absorption spectrum of the transverse plasmon of the gold nanorods indicating that the absorbed photon-to-electron conversion process resulted exclusively in the Au, with the TiO_2 playing a negligible role in charge carrier production. Devices fabricated with 50 nm TiO_2 layers had open-circuit voltages as high as 210 mV, short circuit current densities of 26 μA cm^{-2}, and a fill factor of 0.3. For these devices, the TiO_2 contributed a very small but measurable fraction of the charge carriers.

KEYWORDS: photovoltaics · surface plasmons · gold nanorods · Schottky barrier · TiO_2

The idea behind an all-metal photovoltaic is rather simple. When two metals M1 and M2 for which the work function of M1 (*e.g.*, Au) is greater than that of M2 (*e.g.*, Ti) are brought into contact, they equalize their Fermi levels by electron transfer from M2 to M1. But because both phases are good conductors, the interface does not sustain an internal potential difference. However, if a very thin dielectric or semiconductor layer is interposed between the two metals, creating a metal–insulator–metal (MIM) device, equalization of the chemical potentials occurs across the three phases which renders M1 negative and M2 positive, and a potential difference is created across the thin interstitial layer (Figure 1a). If M1 is a bulk metal, then shining visible or near IR light on it does not create easily separable electrons and holes on account of the facile electron/hole recombination and other scattering events, resulting in negligible photocurrents across the MIM device.[1,2] Moreover, since many of the filled and empty electronic states belong to the same band, momentum conservation considerations would strongly limit the number of allowed transitions. If the two metal layers are sufficiently thin (as compared to the electronic mean-free path and the absorption length of the metal), and light at an appropriate, wavelength-dependent angle of incidence is directed into the device through a prism pressed against the surface of M2, then a surface plasmon polariton can be excited at the metal–air interface of M1 that can produce a measurable, although very small electron excess in M1 over M2 which can produce a current across the device.[3]

* Address correspondence to moskovits@chem.ucsb.edu.

Received for review March 10, 2014 and accepted May 26, 2014.

Published online May 26, 2014
10.1021/nn501379r

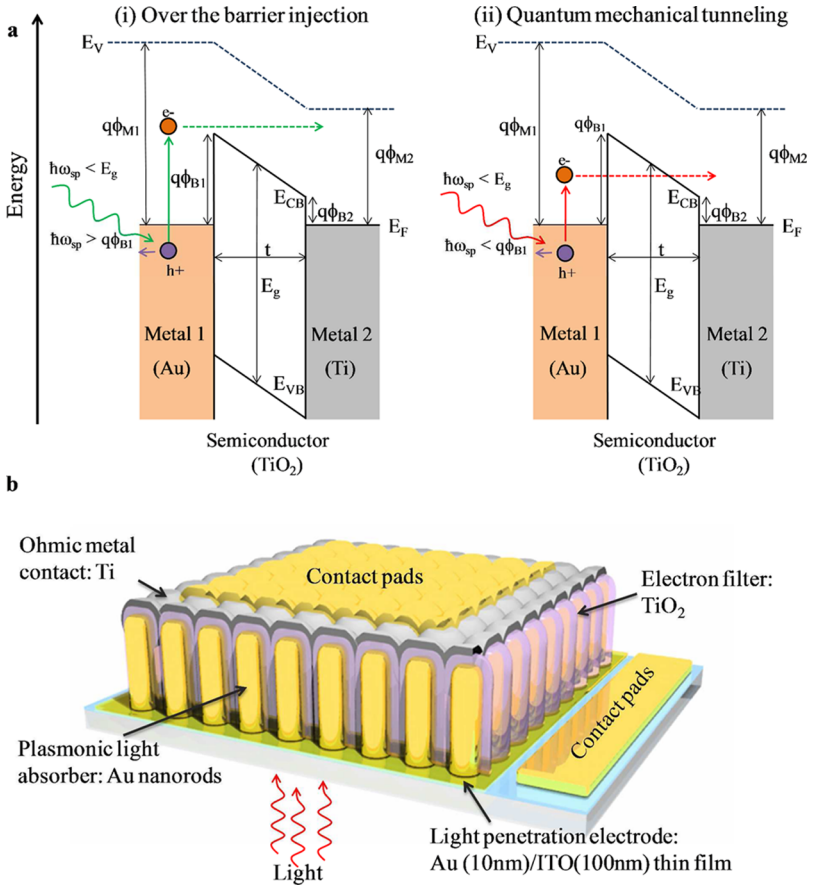

Figure 1. Structure and hot carrier transfer process in the plasmonic photovoltaic device. (a) A schematic showing how excited electrons created by plasmon decay are transmitted as conduction electrons to a contiguous TiO_2 layer. A fraction of the energetic electrons have sufficient energy to directly overcome the Schottky barrier (i). Some quantum mechanically tunnel (ii) through the barrier of width, *t*, to enter the conduction band of TiO_2. The relevant energy levels pertaining to the device structure are shown schematically: the Schottky barrier, $q\phi_B$, the Fermi energy, E_F, and the valence (E_{VB}) and conduction band edges (E_{CB}) of the semiconductor with its band gap, E_g. (b) Artist's conception of the device shown in cross section: the oriented gold nanorod arrays are coated TiO_2 using ALD. Titanium metal (whose work function is less than that of Au) serves as the back contact.

Far greater currents are in principle possible if metal M1 is appropriately nanostructured, for example, by producing it in the form of a two-dimensional array of aligned gold nanorods. This will almost completely lift the momentum conservation restriction allowing visible light to couple with the metal by direct illumination, producing strong localized surface plasmons excitations, which, when illuminated continuously, decay to a large number of hot electrons per second. A significant fraction of these will flow from M1 to M2 under the influence of the internal field. A load connected across the two metals completes the circuit allowing work to be performed. In other words, by following this prescription, one should be able to fabricate a photovoltaic device in which *all* of the charge carriers derive from the metal. Two devices illustrating this principle have recently been reported both of which,[3,4] however, produced very small photocurrents at zero bias for gold based plasmonic devices, and large IPCE values were reported only when the devices were operated with significant forward biases.

(One notes in passing that nanostructuring M1 will, in general, also modify its work function both because high-index planes with varying values of the work function could be created, and also on purely electrostatic grounds. For example, classically, the ionization potential (IP) of a perfectly conducting metal sphere of radius *R* is given by $IP(R) = W + e^2/2R$ in which *W* is the work function of the bulk metal[5] and IP(*R*) functions as the effective work function of an assembly of nanoparticles with radius *R*. A nanosphere with a small radius will, therefore, appear to have a larger work function than the bulk. By nanostructuring the two phases differently, for example, by constructing M1 and M2 out of ensembles of gold nanospheres, with smaller radii in M1 than in M2, one could, in principle, fabricate a photovoltaic, albeit not a very efficient one, using only one metal.)

That plasmon decay can create hot electrons with significant kinetic energies is now fairly well established.[6−8] The energy distributions of such electrons had already been measured in the 1990s,[9] and over

two dozen publications have recently appeared that report a number of photophysical and photochemical processes carried out by plasmonically derived hot electrons, such as (i) photoinduced currents between a plasmonic metal and an adjacent semiconductor;[10−13] (ii) photoelectrocatalytic processes;[14−16] and (iii) photodetection.[17,18]

Here, we report the successful fabrication of a photovoltaic device in which all of the charge carriers: electrons and holes are derived from plasmonic and electronic processes occurring in metals with negligible contribution from its nonmetallic components.

RESULTS AND DISCUSSION

Photovoltaic devices were constructed as a metal−semiconductor Schottky diodes consisting of an array of parallel gold nanorods (~550 nm in length and 90 nm in diameter) coated conformally with TiO_2 films of various thicknesses ranging from 10 to 50 nm laid down by atomic layer deposition (ALD); e-beam deposited titanium forms the lower work-function second metal (M2) and simultaneously as an Ohmic back contact (Figure 1b). A thin film of Au (10 nm) on the ITO serves as an almost-transparent (transmission ~80%) front metal contact (Supporting Information Figure S1). The Au/TiO_2 Schottky junction should have a barrier, ϕ_{SB}, of ~1.0 eV.[19] The plasmon resonances of the gold nanorods occur in the visible and near-infrared, with photon energies far below the band gap of TiO_2 (E_g of anatase = 3.2 eV),[20] so that no significant photocurrent results from the excitation of the semiconductor when the device is illuminated by visible light, and the (transverse) plasmon resonance of the gold nanorods used corresponds approximately to the fluence maximum of the solar spectrum.

The gross features of the dynamics of the hot electrons produced in the Au nanorods pursuant to plasmonic dephasing are fairly well understood.[21,22] Plasmons dephase over a time span of a few femtoseconds creating a shower of electrons that interact adiabatically by electron−electron interactions to form a short-lived energy distribution with a temperature that can reach several thousand Kelvin. Electron−phonon interactions, which operate over times characteristic of nuclear vibrational motion (~1−5 ps), sharply reduce the mean electron temperature over that time span. Hot holes are also formed which quickly migrate to the Fermi surface. Further thermalization with the device's environment then occurs over several hundred picoseconds. This means that an efficient plasmonic solar device must be able to collect and utilize hot electrons within ~5 ps of their generation. Although the above aspects of the hot electron dynamics are rather well understood, a great deal remains unknown regarding the hot electron energy and momentum distributions and their time evolution. Likewise, the properties of the steady state electron energy distribution in a plasmonic system illuminated continuously are not well understood. For example, we do not know what the steady-state concentration of electrons with energies above some threshold energy would be in an ensemble of gold nanorods (such as those used in this study) illuminated by white light in which plasmons are presumably continually excited and decay; and specifically the extent to which normally unfilled levels of the metal's conduction band with energies greater than $\hbar\omega_{SP}$ (the SP photon energy) above the Fermi level. Nevertheless, the number of carriers produced is quite remarkable. Assuming a plasmonic lifetime of 10 fs and 10^{10} nanostructures cm^{-2} (as in our device), and assuming that each plasmonic excitation results in a single hot electron one, one expects over a mole of hot electrons (1 Faraday) to be produced (inside the metal) per second, per cm^2, assuming the surface absorbed a sufficient luminous flux. The challenge is to extract and utilize these carriers.

The steps through which the hot electrons lead to photocurrents are summarized in Figure 1a. Hot electrons that are able to clear the Schottky barrier, or to quantum mechanically tunnel through it into the conduction band of the thin TiO_2 layer, can be conducted to the Ti collector electrode. Since the hot electrons continually lose energy as they thermalize, the electrons that have successfully crossed the interface into the semiconductor will continue to lose their excess energy thereby reducing the probability of their return into the metal. The positive charges that remain in the gold, function as holes, greatly limiting the opportunity for electron−hole recombination. This charge separation produces a photovoltage, whose maximum value will be the work function difference between gold and titanium (~0.9 eV). The hot holes are collected by the Au/ITO contact completing the circuit.

Devices fabricated with 10 nm layers of TiO_2 produced respectable short circuit photocurrents (J_{SC}) in the range 70−120 μA cm^{-2} when illuminated with (simulated) one-sun AM 1.5 light. However, the open circuit voltages (V_{OC}) of these devices were only ~10 mV (Figure 2a) and the devices shorted when a large external bias was applied, likely due to dielectric breakdown of the very thin TiO_2 layer possibly associated with defects. Increasing the TiO_2 layer to 50 nm produced gold-nanorod/TiO_2/Ti devices with stable V_{OC} as high as 210 mV, a J_{SC} of 26 μA cm^{-2}, and a fill factor of 0.3 and a power conversion efficiency of ~0.002% (Figure 2b). The large decrease in current density is likely due to the poor crystallinity of the TiO_2 reducing its conductance, thereby increasing recombination events in the thicker film prior to the electron's reaching the Ti electrode (Supporting Information Figure S2). The wavelength response of the three classes of devices fabricated shows that only for the devices fabricated with 50 nm of TiO_2 does the

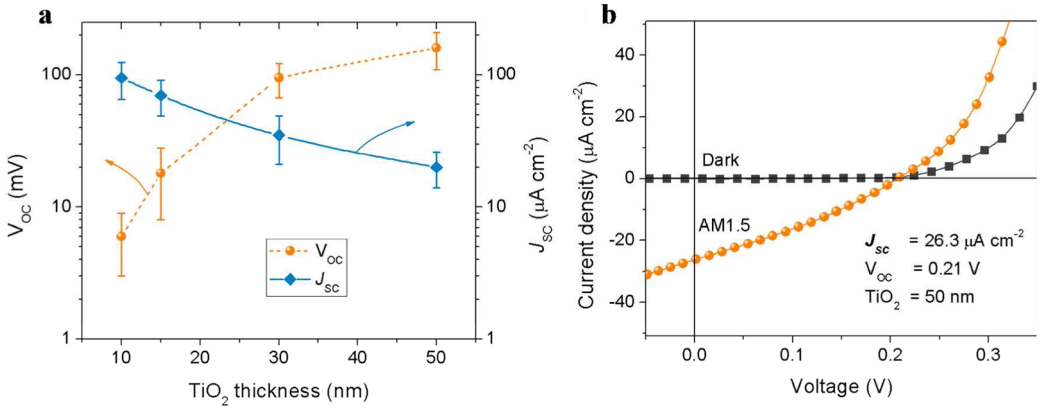

Figure 2. (a) Measured short circuit current densities (J_{sc}) and open circuit voltages (V_{oc}) as a function of the TiO_2 films thickness. The error bars indicate the range of values measured for devices of nominally equal TiO_2 film thickness. Note the logarithmic ordinate scale. (b) Current *vs* voltage response of a plasmonic photovoltaic device based on Au nanorods coated with a conformal 50 nm thick TiO_2 film measured in the dark (black squares), and with one sun (AM 1.5) illumination (orange circles).

semiconductor contribute measurably (~25%) to the device's overall efficiency (Figure 3). With 10 and 30 nm layers of the semiconductor, the TiO_2 contributes, respectively, 5% and 10% to overall device's photocurrent. And with visible light illumination ($\lambda > 420$ nm) only photoprocesses in the metal contribute to the photocurrents in all of the devices. Accordingly, the cell's action is not determined by the semiconductor's bandgap, which for TiO_2 would have limited the cell's response to the ultraviolet, but by the energy constraints related to the metal nanostructure's plasmon resonances.

Our conclusion that the observed photocurrents are almost wholly due to surface-plasmon absorption in the metal is corroborated by photocurrent spectroscopy measurements. The incident photon-to-electron conversion efficiency (IPCE) under short circuit conditions is shown in Figure 3b as a function of wavelength for devices fabricated with 10, 30, and 50 nm TiO_2 layers. For comparison, we include the absorption spectrum of the gold nanorods coated with 10 nm TiO_2 (Figure 3a), determined using an integrating sphere, which shows the expected wavelength shift for the transverse plasmon maximum from ~510 to ~580 nm on coating the Au nanorods with TiO_2 (Supporting Information Figure S3). The Au nanorods also possess a longitudinal plasmon, whose wavelength is sensitive to the Au-NR's aspect ratio. In our Au-NR arrays, that feature occurs at ~1150 nm. We observed no significant photocurrent with illumination in the IR for two reasons: (i) the longitudinal modes cannot be formally excited with light polarized transverse to the rod, as is the case for light incident normal to our device; (ii) more seminally, an 1150 nm plasmon would produce hot electrons with initial energies ≤1.08 eV. During approximately the first one or two picoseconds after the plasmon dephases, an electron energy equilibration is established by e−e interaction. One expects relatively few electrons in that electron-energy distribution to have sufficient energy to overcome the device's ~0.9 eV Schottky barrier. This explains the relatively low current yield due to the excitation of the longitudinal plasmon. Of course, this constraint could be ameliorated were one to use a coating material resulting in a lower Schottky barrier.

We note that IPCE (or external quantum efficiency (EQE)) values larger than those we report have been previously claimed for plasmonically enhanced photodiodes/photoelectrochemical cells[23−27] and for plasmonically enhanced photovoltaics.[3,4] However, for the photoelectrochemical and the plasmonically enhanced photovoltaic cells, those large values were obtained only when the device was forward biased. At zero bias (*i.e.*, when the device functioned as a true power source), the IPCEs we report are the highest yet reported.

The action spectra (Figure 3b) show distinct excitonic features at photon energies corresponding to the absorption spectrum of gold nanorods covered in TiO_2, consistent with the mechanism summarized in Figure 1a, and indicate that only electrons produced as a result of surface plasmon decay contribute to the photocurrents measured with visible light. The IPCE values measured at ~580 nm increase dramatically with decreasing the TiO_2 layer thickness (J_{SC} = 110 μA cm^{-2} (IPCE ~ 1.0%) for a device with 10 nm of TiO_2; and J_{SC} = 26 μA cm^{-2} (IPCE ~ 0.23%) for one with 50 nm of TiO_2, implying an increased extraction efficiency of hot electrons with decreasing TiO_2 thickness (Figure 2a). This observation also suggests that improving the crystallinity of the TiO_2 should lead to improved collection of hot electrons over what is possible with the amorphous films produced by ALD.[28] It also suggests the possibility of finding insulator or semiconductor materials with better "electron filtering" performance than TiO_2. The near constancy with increasing TiO_2 thickness of IPCE for illumination wavelengths in the range 300−400 nm (*i.e.*, when $\hbar\omega > E_{g,TiO2}$) is consistent with our reasoning that the major

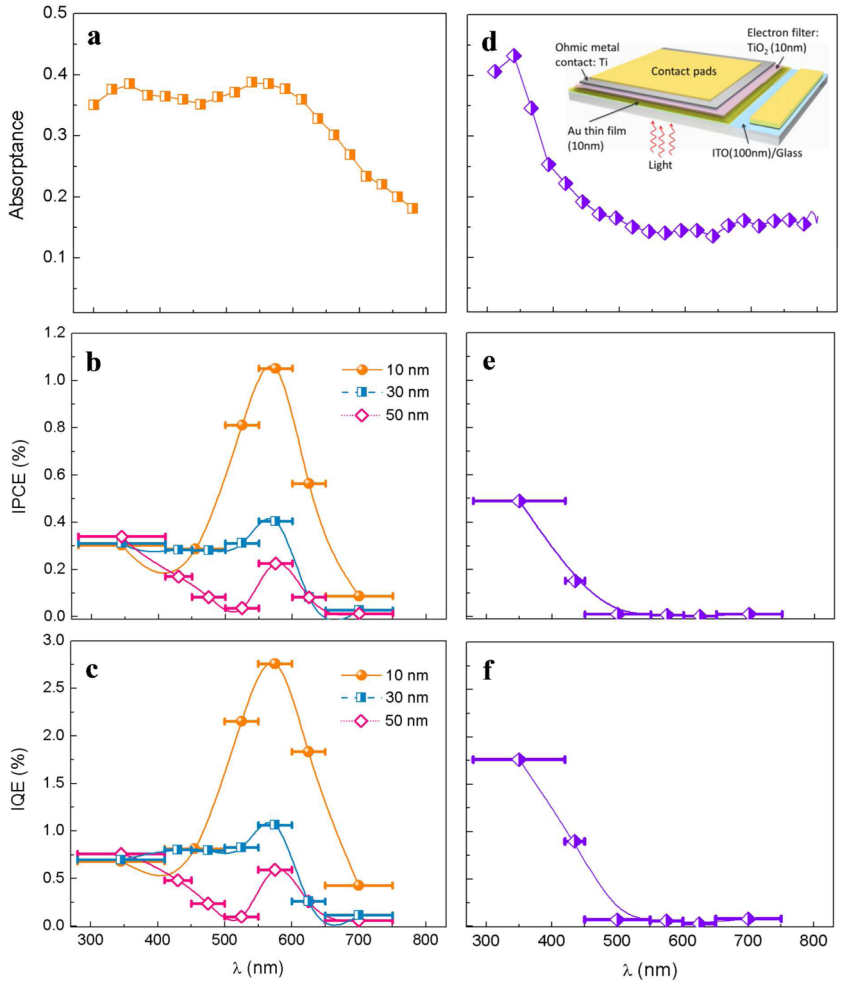

Figure 3. Extinction spectra and wavelength dependent photoresponse of plasmonic photovoltaic device. (a) The absorption spectrum of gold nanorod arrays capped with 10 nm ALD-deposited TiO_2 film (orange squares) on a ~100 nm thick ITO coated glass substrate, measured by separating the absorptance from the transmittance and both specular and diffuse reflectance in an integrating sphere. (b) Incident photon-to-electron conversion efficiency (IPCE) spectra plotted as a function of wavelength of the incident light, of devices fabricated with TiO_2 layers of varying thickness (*t*): (i) 10, (ii) 20, and (iii) 50 nm. The IPCE values were determined by using wavelength cutoff filters. The number of incident photons in each wavelength tranche was measured with a calibrated Si photodiode. The IPCE value is plotted as the solid square in the center of each tranche, while the cutoff wavelengths of the two adjacent cutoff filters that defined the wavelength tranche are shown as solid horizontal lines. (c) Internal quantum efficiency (IQE) spectra as a function of wavelength plotted for devices with TiO_2 thickness (*t*) (i) 10, (ii) 20, and (iii) 50 nm. The IQE reflects the absorbed photon-to-hot-electron injection and collection efficiency of the device. The right-hand panel shows: (d) the absorption spectrum of a 10 nm gold film deposited on ITO, then covered with 10 nm of ALD-deposited TiO_2 followed by 50 nm of Ti metal (device schematic is inset in (d)) with corresponding (e) IPCE and (f) IQE spectrum. All measurements were carried out at zero bias.

causes of carrier loss are unfavorable recombination and scattering events occurring in the TiO_2 layers. Negligible photocurrents were measured for photon energies, $q\phi_{SB} < \hbar\omega < \hbar\omega_{SP}$ ruling out internal photoemission as a major contribution for observed photocurrents.[29] Finally, the short-circuit photocurrents produced are determined largely by the photon capture efficiency, and by the internal quantum efficiency, IQE, defined as the number of hot electrons injected from the plasmonic metal into the semiconductor per absorbed photon, assuming all the injected electrons are collected at the contacts (Figure 3c). IQE is evaluated by dividing IPCE by the fraction of incident photons absorbed by the gold nanorods at a given wavelength. For gold nanorod devices coated with 10 nm TiO_2 layers, the maximum IQE was ~2.75%. It is worth noting that in contrast to semiconductor-based PV cells, where the IQE is weakly dependent on wavelength, the IQE of a plasmonic device is more strongly wavelength dependent. We believe this is because the absorption spectrum of our device (Figure 3a) contains two types of contributions: a short wavelength absorptance (at ~350 nm) that is dominated by direct single-electrons absorptions, *i.e.* band to band absorptions in the TiO_2 and interband transitions in the gold, and the 550 nm absorption due to the plasmon. The observed IQE *vs* wavelength data (Figure 3c) suggests that for the devices with the thinnest TiO_2 layer, the former are not as efficient as the latter in producing extractable carriers. In a normal

photovoltaic, all of the current results from band to band transitions and therefore result in photocurrents with greater uniformity of efficiency.

That plasmonic production of hot electrons increases the IQE values dramatically is demonstrated by comparing the performance of our Au nanorod device to a metal−insulator−metal (MIM) device of similar construction but using a continuous gold film. Figure 3e,f report the IPCE and IQE values for such a nonplasmonic MIM device (depicted schematically in the inset to Figure 3d) constructed using a 10 nm Au thin film capped with 10 nmTiO_2 layer (see Methods section). The device's IPCE and IQE values are very low across all wavelengths with a maximum IPCE of 0.5% and IQE of 1.5% observed at $\hbar\omega > E_g$. Its absorption spectrum (Figure 3d) shows strong absorptions only at wavelengths shorter than ~400 nm where the band-to-band ($\hbar\omega > E_g$) absorptions by the TiO_2, and the (mostly d to sp) interband transitions of the gold occur. It is hard to determine the relative contribution of the gold and the TiO_2 to the observed IQE in the <400 nm region. However, the low value of IQE for $\hbar\omega > E_g$ implies that to whatever extent the TiO_2 contributes to the photocurrent its energy conversion efficiency is very low, likely on account of its poor crystallinity. Continuing this line of reasoning in regard to the IQE values of the plasmonic devices (Figure 3c) for wavelengths shorter than 400 nm, and noting that the IQE values in that spectral region does not scale with the thickness of the TiO_2 layer used, one concludes that the gold nanorods contribute a fraction of the photocurrent in these devices even in the wavelength region $\lambda < 400$ nm.

We note in passing that the plasmonic solar cells reported here showed significant stability against photo-oxidation and high ambient humidity. Figure 4 shows the current−voltage response of plasmonic gold nanorod solar cells coated with 50 nm of TiO_2 at simulated one-sun AM 1.5 illumination after 30 days of open-circuit exposure to ambient atmosphere and lighting. The cell showed less than 8% decrease in short circuit current, and the open-circuit potential actually rose by ~5% during the aging period. This translated in a decrease in overall power conversion efficiency of only ~5% following a month-long aging test. Soaking the device in DI water for 24 h at open-circuit conditions resulted in less than 10% reduction in the overall power conversion efficiency. The devices' response to environmental challenges contrasts with the behavior of traditional (and organic) photovoltaics for which atmospheric humidity often dramatically reduces efficiency.

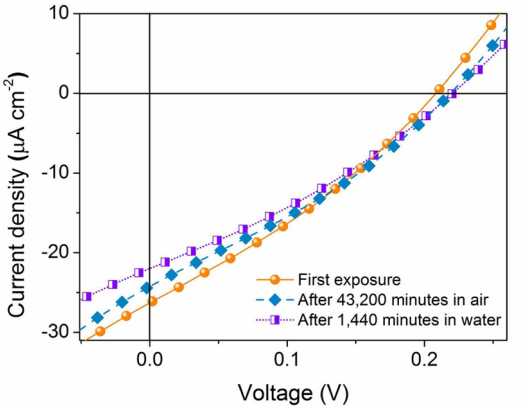

Figure 4. Current *vs* voltage response at simulated one-sun AM1.5 illumination for a typical plasmonic photovoltaic device (Au nanorods conformally coated with a 50 nm thick TiO_2 film) upon first exposure to light, after 43 200 min of exposure to ambient atmosphere and light and after 1440 min of water soaking at open circuit conditions.

CONCLUSIONS

We report a plasmonic photovoltaic device in which the majority of charge carriers are derived from the excitation of surface plasmons in gold nanorods that operates like a traditional photovoltaic delivering power into a load without the assistance of a forward bias and characterized by respectrable values of open-circuit voltage, short-circuit current and fill factor. The device consists of a dense array of vertically oriented gold nanorods ALD-coated with a thin layer of a wide-band gap oxide (TiO_2) and a low work function metal (Ti). Under short circuit conditions, these cells extract hot-electrons with visible wavelength IPCE values of ~1.0% and IQE of 2.75%, considerably higher than what has been reported previously for plasmonic photovoltaics under zero-bias conditions. The cells show noteworthy stability in accelerated aging tests. The short-circuit current densities and open-circuit potential depend markedly on the oxide layer quality and thickness, pointing the way to future strategies for improving the devices' performance, that would lead to the construction of "all-metal" photovoltaics with significant power conversion efficiencies.

METHODS

Device Fabrication. Devices were fabricated on gold (10 nm) coated ITO substrates, which served as the Ohmic front contact through which light is incident. The gold front electrode absorbed (and therefore wasted) approximately 15% of the incident radiant energy. The fabrication method of gold nanorod arrays using templated electrodeposition was reported previously.[30] Briefly, high purity, 1 μm thick, aluminum films were e-beam deposited on Au/ITO substrates, then electrochemically anodized to form porous aluminum oxide (PAO) with pores averaging ~30 nm diameter.[31] The pores were widened to a final diameter of ~100 nm in 5 wt % phosphoric acid, which also completely removed the barrier layer at the alumina/aluminum interface, thereby facilitating DC metal electrodeposition. Gold nanorods (rod lengths ~500−550 nm) were electrodeposited inside the pores. The alumina matrix

was removed by chemical etching and the gold nanorod array was conformally coated using atomic layer deposition (ALD) with TiO_2 films ranging from 10 to 50 nm in thickness. Prior to ALD deposition, the gold nanorods were subjected to an O_2 plasma treatment for 2 min at 100 mW. ALD of TiO_2 was carried out in an Oxford FlexAl ALD tool at 200 °C using tetrakis-(dimethylamino)titanium (TDMAT) and water as precursor and reactant, respectively. Devices were annealed at 500 °C for 60 min under ambient atmosphere to improve the crystallinity of the TiO_2. A 50 nm thick layer of titanium, which functioned as metal M2, and 50 nm thick gold film that served as the Ohmic back contact were e-beam deposited through a shadow mask. For a nonplasmonic MIM device, 10 nm gold film was e-beam evaporated on ITO/glass substrates at a rate of 0.1 Å/s followed by ALD deposition of 10 nm TiO_2 film. The device was then capped with 50 nm titanium and 100 nm gold to form Ohmic metal back contact. The ITO serves as the transparent front contact.

Device Characterization. The photoresponse of the devices was evaluated under 100 mW cm^{-2} standard air mass 1.5 global (AM 1.5) sunlight with cells placed on a controlled temperature block to reduce heating. The light source was a 300 W xenon arc lamp. Intensities were determined using a calibrated Si photodiode. A 0.1 cm^2 shadow mask that limits the beam size to an area smaller than the area of back contacts (0.2 cm^2) was carefully aligned between the light source and the solar cell; this defined the active area of the device. Current–voltage curves were measured using a Keithley power supply at a voltage ramp rate of 0.01 V/s. IPCE was estimated using a set of cutoff optical filters with varying short-wavelength cutoff, by measuring the current density under short circuit conditions and the photon flux for each wavelength region using the calibrated Si photodiode. The IQE was estimated using absorption measurements deduced from the transmission and (specular plus diffuse) reflectance spectra of the device measured using an integrating sphere and fiber-optic coupled monochromator.

Conflict of Interest: The authors declare no competing financial interest.

Supporting Information Available: Schematic of the energy structure, extinction spectrum and discussion on hot electrons derived from surface plasmon excitations. This material is available free of charge *via* the Internet at http://pubs.acs.org.

Acknowledgment. This work was supported by the MRSEC Program of the National Science Foundation under Award No. DMR 1121053, and made extensive use of the MRL Central Facilities at UCSB, a member of the NSF-funded Materials Research Facilities Network (www.mrfn.org). The authors gratefully acknowledge research support from the Institute for Energy Efficiency, an Energy Frontier Research Center funded by the U.S. Department of Energy, Office of Science, Office of Basic Energy Sciences, Award Number: DE-SC0001009. N.S. is supported by the ConvEneIGERT Program (NSF-DGE 0801627). The authors also acknowledge Prof. Eric W. McFarland for helpful suggestions on IPCE and IQE measurements and calculations.

REFERENCES AND NOTES

1. Thon, A.; Merschdorf, M.; Pfeiffer, W.; Klamroth, T.; Saalfrank, P.; Diesing, D. Photon-Assisted Tunneling *versus* Tunneling of Excited Electrons in Metal–Insulator–Metal Junctions. *Appl. Phys. A: Mater. Sci. Process.* **2004**, *78*, 189–199.
2. Sze, S. M.; Ng, K. K. Metal-Semiconductor-Metal Photodetector. In *Physics of Semiconductor Devices*, 3rd ed.; John Wiley & Sons, Inc.: Hoboken, NJ, 2007; pp 712–716.
3. Wang, F.; Melosh, N. A. Plasmonic Energy Collection through Hot Carrier Extraction. *Nano Lett.* **2011**, *11*, 5426–5430.
4. Garcia de Arquer, F. P.; Mihi, A.; Kufer, D.; Konstantatos, G. Photoelectric Energy Conversion of Plasmon-Generated Hot Carriers in Metal–Insulator–Semiconductor Structures. *ACS Nano* **2013**, *7*, 3581–3588.
5. Makov, G.; Nitzan, A.; Brus, L. E. On the Ionization Potential of Small Metal and Dielectric Particles. *J. Chem. Phys.* **1988**, *88*, 5076–5085.
6. Hofmann, J.; Steinman, W. Plasma Resonance in the Photoemission of Silver. *Phys. Status Solidi B* **1968**, *30*, K53–K56.
7. Bösenberg, J. Photoelectrons from Optically Excited Nonradiative Surface Plasma Oscillations. *J. Phys. Lett. A* **1971**, *37*, 439–440.
8. Daboo, C.; Baird, M. J.; Hughes, H. P.; Apsley, N.; Jones, G. A. C.; Frost, J. E. F.; Peacock, D. C.; Ritchie, D. A. Surface-Plasmon-Enhanced Photodetection in Planar Au-GaAs Schottky Junctions. *Thin Solid Films* **1990**, *189*, 27–38.
9. Shalaev, V. M.; Douketis, C.; Stuckless, J. T.; Moskovits, M. Light-Induced Kinetic Effects in Solids. *Phys. Rev. B* **1996**, *53*, 11388–11402.
10. Tian, Y.; Tatsuma, T. Mechanisms and Applications of Plasmon-Induced Charge Separation at TiO_2 Films Loaded with Gold Nanoparticles. *J. Am. Chem. Soc.* **2005**, *127*, 7632–7637.
11. Neretina, S.; Qian, W.; Dreaden, E.; El-Sayed, M. A.; Hughes, R. A.; Preston, J. S.; Mascher, P. Plasmon Field Effects on the Nonradiative Relaxation of Hot Electrons in an Electronically Quantized System: CdTe–Au Core–Shell Nanowires. *Nano Lett.* **2008**, *8*, 2410–2418.
12. Mubeen, S.; Hernandez-Sosa, G.; Moses, D.; Lee, J.; Moskovits, M. Plasmonic Photosensitization of a Wide Band Gap Semiconductor: Converting Plasmons to Charge Carriers. *Nano Lett.* **2011**, *11*, 5548–5552.
13. Knight, M. W.; Wang, Y.; Urban, A. S.; Sobhani, A.; Zheng, B. Y.; Nordlander, P.; Halas, N. J. Embedding Plasmonic Nanostructure Diodes Enhances Hot Electron Emission. *Nano Lett.* **2013**, *13*, 1687–1692.
14. Sun, M.; Xu, H. A Novel Application of Plasmonics: Plasmon-Driven Surface-Catalyzed Reactions. *Small* **2012**, *8*, 2777–2786.
15. Chen, H. M.; Chen, C. K.; Chen, C. J.; Cheng, L. C.; Wu, P. C.; Cheng, B. H.; Ho, Y. Z.; Tseng, M. L.; Hsu, Y. Y.; Chan, T. S.; *et al.* Plasmon Inducing Effects for Enhanced Photoelectrochemical Water Splitting: X-ray Absorption Approach to Electronic Structures. *ACS Nano* **2012**, *6*, 7362–7372.
16. Mubeen, S.; Lee, J.; Singh, N.; Krämer, S.; Stucky, G. D.; Moskovits, M. An Autonomous Photosynthetic Device in Which All Charge Carriers Derive from Surface Plasmons. *Nat. Nanotechnol.* **2013**, *8*, 247–251.
17. Knight, M. W.; Sobhani, H.; Nordlander, P.; Halas, N. J. Photodetection with Active Optical Antennas. *Science* **2011**, *332*, 702–704.
18. Fang, Z.; Liu, Z.; Wang, Y.; Ajayan, P. M.; Nordlander, P.; Halas, N. J. Graphene-Antenna Sandwich Photodetector. *Nano Lett.* **2012**, *12*, 3808–3813.
19. McFarland, E. W.; Tang, J. A Photovoltaic Device Structure Based on Internal Electron Emission. *Nature* **2003**, *421*, 616–618.
20. Tang, H.; Prasad, K.; Sanjinès, R.; Schmid, P. E.; Lévy, F. Electrical and Optical Properties of TiO_2 Anatase Thin Films. *J. Appl. Phys.* **1994**, *75*, 2042–2047.
21. Ahmadi, T. S.; Logunov, S. L.; El-Sayed, M. A. Picosecond Dynamics of Colloidal Gold Nanoparticles. *J. Phys. Chem.* **1996**, *100*, 8053–8056.
22. Sönnichsen, C.; Franzl, T.; Wilk, T.; von Plessen, G.; Feldmann, J.; Wilson, O.; Mulvaney, P. Drastic Reduction of Plasmon Damping in Gold Nanorods. *Phys. Rev. Lett.* **2002**, *88*, 0774021–07740214.
23. Nishijima, Y.; Ueno, K.; Yokota, Y.; Murakoshi, K.; Misawa, H. Plasmon-Assisted Photocurrent Generation from Visible to Near-Infrared Wavelength Using a Au-Nanorods/TiO_2 Electrode. *J. Phys. Chem. Lett.* **2010**, *1*, 2031–2036.
24. Lee, Y. K.; Jung, C. H.; Park, J.; Seo, H.; Somorjai, G. A.; Park, J. Y. Surface Plasmon-Driven Hot Electron Flow Probed with Metal-Semiconductor Nanodiodes. *Nano Lett.* **2011**, *11*, 4251–4255.
25. Reineck, P.; Lee, G. P.; Brick, D.; Karg, M.; Mulvaney, P.; Bach, U. A Solid-State Plasmonic Solar Cell *via* Metal Nanoparticle Self-Assembly. *Adv. Mater.* **2012**, *24*, 4750–4755.

26. Takahashi, Y.; Tetsu, T. Solid State Photovoltaic Cells Based on Localized Surface Plasmon-Induced Charge Separation. *Appl. Phys. Lett.* **2011**, *99*, 182110.
27. Lee, H.; Lee, Y. K.; Hwang, E.; Park, J. Y. Enhanced Surface Plasmon Effect of Ag/TiO_2 Nanodiodes on Internal Photoemission. *J. Phys. Chem. C* **2014**, *118*, 5650–5656.
28. Abaffy, N. B.; McCulloch, D. G.; Partridge, J. G.; Evans, P. J.; Triani, G. Engineering Titanium and Aluminum Oxide Composites Using Atomic Layer Deposition. *J. Appl. Phys.* **2011**, *110*, 123514(1)–123514(8).
29. Helman, J. S.; Sánchez-Sinencio, F. Theory of Internal Photoemission. *Phys. Rev. B* **1973**, *7*, 3702–3706.
30. Lee, J.; Mubeen, S.; Ji, X.; Stucky, G. D.; Moskovits, M. Plasmonic Photoanodes for Solar Water Splitting with Visible Light. *Nano Lett.* **2012**, *12*, 5014–5019.
31. Lee, S. J.; Guan, Z.; Xu, H.; Moskovits, M. Surface-Enhanced Raman Spectroscopy and Nanogeometry: The Plasmonic Origin of SERS. *J. Phys. Chem. C* **2007**, *111*, 17985–17988.